**International Journal of Smart Energy Technology and Environmental Engineering**
**Volume 3, Issue 1, March 2024**
https://setee.globalpublisher.org/
http://globalpublisher.org/journals-1007/

# Experimental investigation of hydrogen fueled Wankel engine from the point of view of relationship between knock, flame velocity, flow velocity and combustion velocity.

**Seyed Karim Sharifi[1,*], Mohammad Azarshab[2], Ali Khoshnam[3]**
1- Independent researcher – Turbomachinery and automotive expert
2- Damoon choob mandegar – Mechanical engineer (manufacturing engineering)
3- Independent researcher – Mechanical expert (fixed and rotating equipments)
* Corresponding Author: sharifi.s.k19@gmail.com

## ABSTRACT

Environmental issues have increased the importance of developing pollution-free internal combustion engines. In this article, the necessity of using twin spark plugs, the effect of excess air ratio with changing the flame velocity on the ignition velocity and the effect of the engine speed with changing the flow velocity on the HWRE ignition velocity and its effect on the flame velocity are stated. Flame velocity and flow velocity are positively correlated to knock intensity, and flow velocity has a more significant effect.

**Keywords:** Wankel rotary engine (WRE), Hydrogen-fueled Wankel rotary engine (HWRE), Internal combustion engine (ICE), Reciprocating piston engine (RPE), Knock intensity (KI), Bottom dead center (BDC), Top dead center (TDC) After bottom dead center (ABDC), After top dead center (ATDC), Before bottom dead center (BBDC), Before top dead center (BTDC) Backward combustion velocity (BCV), Forward combustion velocity (FCV) Electronic control unit (ECU), Leading spark plug (LSP), Trailing spark plug (TSP), Manifold absolute pressure (MAP), Spark ignition (SI), Crank angle (◦CA), flame velocity, flow velocity, combustion velocity, dual spark plug, hydrogen, fuel

## 1. INTRODUCTION

Wankel Rotary Engine Due to its simple structure, compact layout and high power-to-weight/volume ratio, WRE has significant powertrain advantages. However, the elongated combustion chamber of the WRE amplifies the negative effects of quenching and the high

velocity unidirectional flow in the combustion chamber reduces the combustion efficiency, both of which underperform the fossil-fueled WRE.

Hydrogen fuel does not emit carbon and corresponds to the theme of carbon neutrality. And some physicochemical properties of hydrogen, such as wide flammability limits that allow increased thermal efficiency by lean combustion and etc., make it suitable as a fuel for internal combustion engines (ICEs). WRE will perform better using hydrogen fuel from reciprocating piston engines (RPEs). On the one hand, short quenching distance and fast combustion velocity are beneficial to improve the combustion efficiency of WRE; on the other hand, the compact structure and high power density can cover more distance and produce more power. According to the studies, HWRE is not prone to occur backfire, but it is more likely to occur in RPEs. In addition, the compact structure of the WRE also compensates for the disadvantage of the large hydrogen storage device. However, limited to the elongated combustion envelope and non-uniform thermal load, the knock in HWREs is more severe compared to hydrogen-fueled RPEs.

Knock as an abnormal combustion in spark ignition (SI) engines mainly manifests as high combustion temperature, abnormal in-cylinder pressure profiles and very fast flame propagation velocity. Knock as an abnormal combustion in spark ignition (SI) engines mainly manifests as high combustion temperatures, abnormal in-cylinder pressure profiles, and extremely fast flame propagation speeds, which usually leads to low efficiency, poor propagation and even structural damage. Due to differences in fuel properties, knocking in gasoline-fueled ICEs is usually caused by end-gas spontaneous combustion, while hydrogen-fueled ICE knocking is usually caused by rapid and unstable combustion and sometimes end-gas spontaneous combustion. The knock caused by the rapid and unstable combustion of hydrogen occurs simultaneously with the combustion caused by the spark plug and goes through all the stages of combustion. High knock intensity is usually associated with short combustion duration. The occurrence of knock with main flame acceleration up to 400 m/s is due to the rapid combustion of the main flame, and the occurrence of knock due to autoignition of the end gas is well correlated to the combustion velocity of the main flame, because this knock occurs in the hottest region of the end gas, which where the temperature depends mainly on the pressure increase produced by the combustion. In summary, regular flame propagation plays an important role in the occurrence of knock, and one should consider isolated effects of knock and special phenomena, such as autoignition. In particular, for hydrogen-fueled ICEs, knock occurs during the combustion process.

Due to differences in structure and mode of operation, the flame emission of WREs is significantly differentiated from that of RPEs. In RPEs, there will be a vortex or swirl near top dead center (TDC), while in WREs, the direction of the flow field is essentially consistent with the tangential direction of rotor rotation and there is no vortex or swirl. Therefore, the flame propagation has different effects on the knock level based on the flow field.

This paper presents a method for measuring combustion, flame and flow velocity of WRE using experimental instruments and quantifying them with knock level in HWRE.

## 2. Experimental facilities and named parameters

### 2.1. Experimental facilities

To measure the combustion velocity, a WRE with dual spark plug has been used. As shown in Fig. 1, According to the direction of rotation of the rotor, the spark plug in front of the minor axis is named leading spark plug (LSP) and the plug behind the minor axis is named trailing spark plug (TSP). The distance from LSP and TSP to the minor axis is 23 and 30 mm respectively, that is, the distance between them is 53 mm.

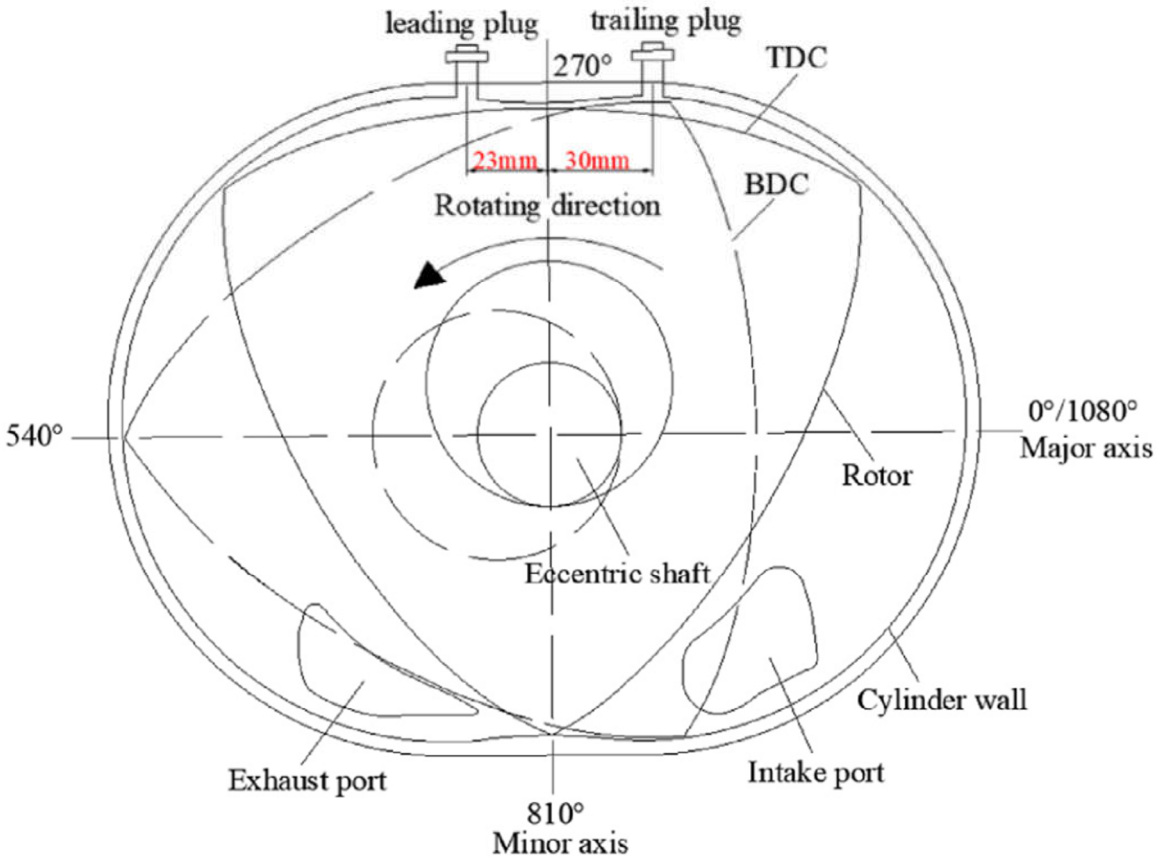


**Fig. 1.** The structural schematic of the tested WRE. [43]

**Table 1.** Engine specification.

| Specification | Value |
|---|---|
| Number of rotors | 2 |
| Cooling method | Water cooling |
| Ignition source | Dual spark plug |
| Intake method | Side-ported natural aspiration |
| Exhaust method | Side port |
| Generating radius/mm | 105 |
| Width of rotor/mm | 80 |
| Displacement/L | 0.654L |
| Compression ratio | 10 |
| Eccentricity/mm | 15 |
| Intake timing/(◦CA) | 3◦ ATDC, 38◦ ABDC |

| | |
|---|---|
| Exhaust timing/(◦CA) | 80◦ BBDC, 3◦ BTDC |

The tested WRE is initially fueled by gasoline. Hence, to meet experimental requirements, some preliminary work must be done: (1) A self-developed port-injected hydrogen supply system was installed to replace the original gasoline supply system. The supply pressure of hydrogen was fixed at 5 bar; (2) A self-developed electronic control unit (ECU) was used to control the ignition timing and hydrogen supply amount per cycle. The self-developed ECU intercepts the ignition and injection signals from the original ECU and controls the ignition and injection for the next cycle of HWRE in conjunction with the crank position signal; (3) Some sensors were installed to measure some requisite parameters, such as intake pressure sensor, in-cylinder pressure sensor, oxygen sensor and so on.

The Kistler 6117BFD17 piezoelectric sensor (measurement uncertainty: ≤ ±0.3 bar) installed on the LSP measures the in-cylinder pressure, which is the most important parameter. The Powerlink CAC6 AC dynamometer (measurement uncertainty: speed ≤ ±1 rpm and load ≤ ±0.4% F.S) controlled engine speed and throttle percentage (load). The in-cylinder pressure profile was shown on the computer by the Kibox. The experimental system schematic is shown in Fig. 2, which includes some facilities not used in this work.

1. Air cleaner 2. Mass flow meter of air 3. Container of hydrogen 4. Pressure regulating valve of hydrogen 5. Pressure meter of hydrogen 6. Hydrogen flow displayer 7. Volumetric flowmeter of hydrogen 8. Backfire arrestor of hydrogen 9. Smart gas box 10. Injector of hydrogen 11. HECU (Hydrogen Electronic Control Unit) 12. Calibration computer 13. Kibox 14. Trailing plug 15. Leading plug 16. Charger amplifier 17. Analog-digital converter 18. Exhaust sampling 19. Emissions analyzer 20. Oxygen sensor 21. Lambda analyzer a1. Data signals from HECU to calibration computer a2. Control signals from calibration computer to HECU b. Signals from sensors to HECU.

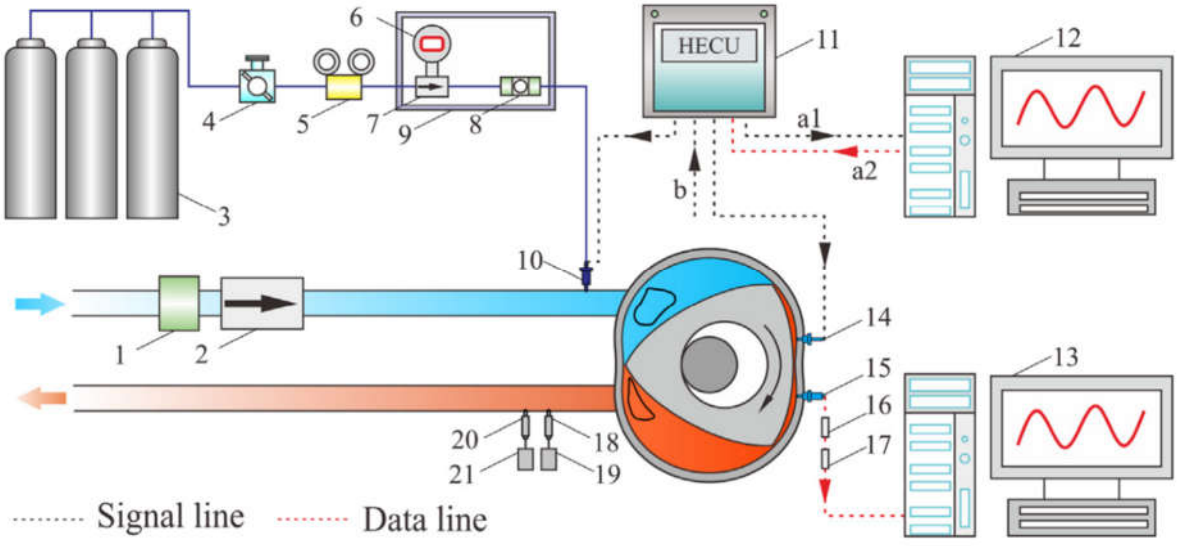


**Fig. 2.** The schematic diagram of the experiment system. [43]

### 2.2. Parameters named

The desired parameters in this research are flow velocity, combustion velocity and flame velocity. The flow velocity is the average velocity of the flow field inside the cylinder; The combustion velocity is the average velocity of flame propagation under the effect of the flow field; The flame velocity is the average flame propagation velocity that decoupling the flow field. Since the flow field in the WRE near TDC is essentially unidirectional tangential to the rotor, the three velocities mentioned above can be considered unidirectional and non-rotating near TDC. Moreover, without considering the vertical direction of the rotor, since the flow is unidirectional while the flame propagation is bidirectional, as shown in Fig. 3, which is the schematic representation of flow velocity and combustion velocity, two parameters, forward combustion velocity (FCV) and backward combustion velocity (BCV), were also introduced in this work. Based on the above descriptions, two equations (1) and (2) are obtained:

FCV = Flame velocity + Flow velocity (1)
BCV = Flame velocity - Flow velocity (2)

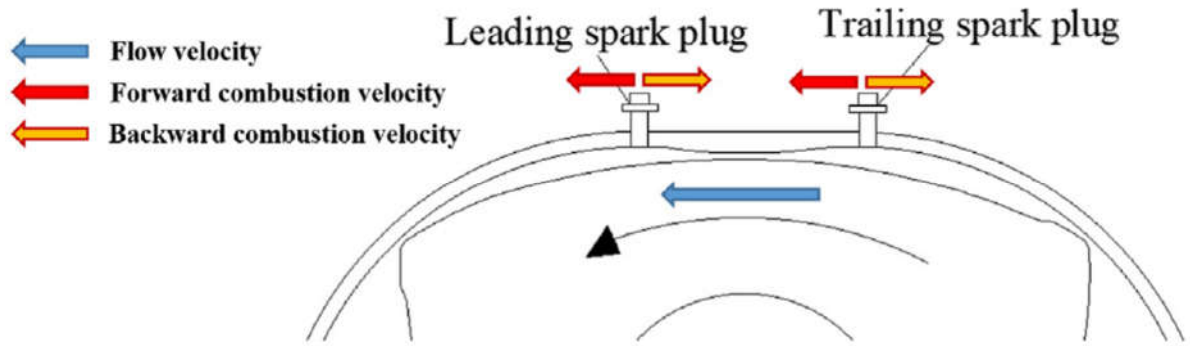


**Fig. 3.** The schematic of flow velocity and combustion velocity. [43]

A band-pass filter is used to extract the knock characteristic. To extract the knock feature, a band-pass filter is used, which can remove the low-frequency normal ignition signal and the high-frequency noise. The passband cutoff frequency of this filter is set as 3-20 kHz. Fig. 4 shows the pressure inside the cylinder and the respective knock pressure, which is the result of the processing of band-pass filter. To quantify the knock level, the knock intensity (KI) is introduced, which indicates the magnitude of the peak-to-peak knock pressure. Therefore, KI can be expressed by equation (3):

KI = knock pressure (max) - knock pressure (min) (3)

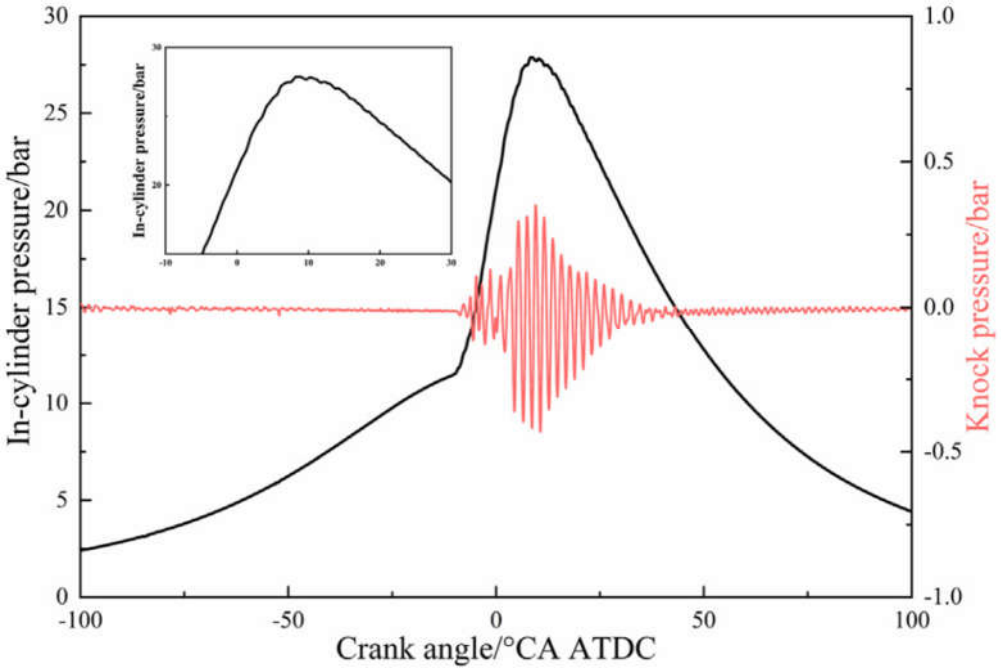


**Fig. 4.** The in-cylinder pressure and corresponding knock pressure. [43]

## 3. Results and discussion

### 3.1. Combustion velocity measuring methodology

A method for measuring WRE combustion velocity with hydrogen fuel was proposed, which is theoretically applicable for other fuels of this engine as well. To measure FCV, fix the TSP ignition timing at -12◦CA ATDC and gradually delay the LSP ignition timing from -12◦ CA ATDC in 1◦ CA intervals. Because the LSP ignition timing is delayed, the average in-cylinder profiles of 300 consecutive cycles at different LSP ignition timings and a constant -12◦CA ATDC ignition timing of the TSP at 1000 rpm are displayed, According to Fig. 5. The in-cylinder pressure changes, but when the LSP ignition timing is later than -6◦CA ATDC, the in-cylinder pressure is the same, which indicates that at this situation, the flame produced by the TSP propagated past the LSP and the LSP spark is meaningless. The distance (d) between two spark plug is 53 mm. which is 6◦CA in the case of Fig. 5. Therefore, FCV can be calculated with the following equation:

$$FCV = \frac{d}{\frac{\Delta t}{360}\Big/\frac{n}{60}} \quad (4)$$

Δt is the ignition interval between two spark plugs. n is the engine speed and is equal to 1000 r/min. Hence, by calculation, when the HWRE operates at 80 kPa manifold absolute pressure (MAP), stoichiometric ratio and engine speed of 1000 r/min, the FCV is 53 m/s.

The difference between BCV and FCV measurement is that the roles of LSP and TSP must be switched. The error of this method is mainly caused by the tested ignition timing

interval to change the spark plug, and if the ignition timing interval is set as 1◦ CA, the error can be considered as ±1◦ CA.

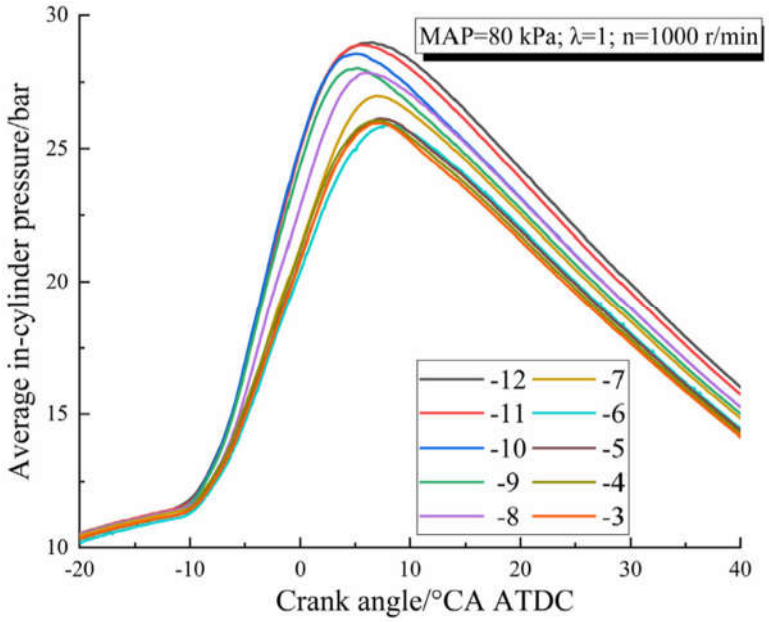


**Fig. 5.** The in-cylinder pressure at different ignition timings of LSP at 1000 r/min. [43]

### 3.2. Combustion, flow and flame velocity

3.2.1. Excess air ratio

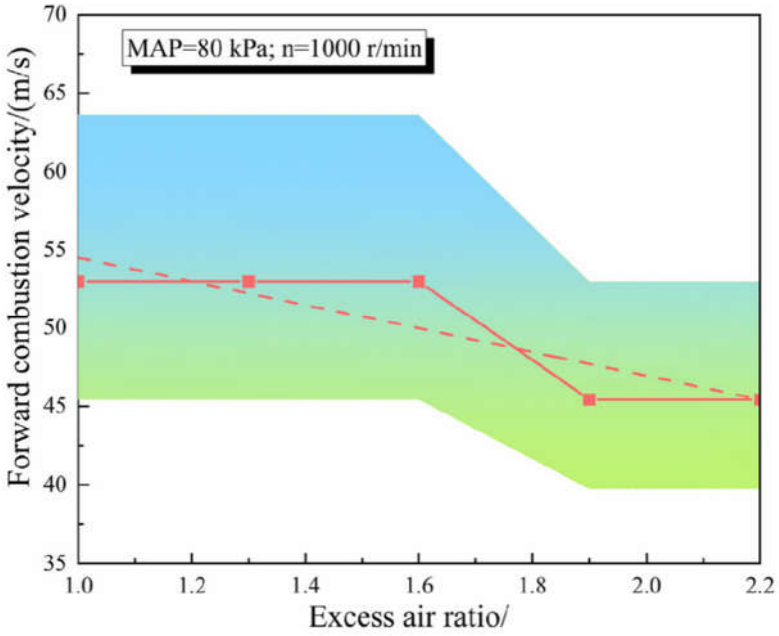


**Fig. 6.** The forward combustion velocity at different excess air ratios. [43]

Fig. 6 shows the FCV at different excess air ratios, which includes measured data (dotted line), fitted data (dashed line) with 0.75 $R^2$ and error band (colored band). Limited by the self-developed ECU, the minimum adjustable step length of ignition timing is 1◦CA, so when the

FCV does not change significantly, its test value is the same. It can be seen from Fig. 6 that with increasing the excess air ratio, the change of FCV has a declining tendency, which can be explained by the following reason: when the engine speed and MAP are maintained, the basically constant flow field is not responsible for the variation of FCV. The fastest hydrogen laminar flame velocity is achieved at an excess air ratio of approximately 0.6 (equivalence ratio of 1.7). As the excess air ratio increases from 0.6, which decreases the charge, the laminar flame velocity decreases gradually, which is also true for turbulent combustion and can be used for qualitative analysis of turbulent combustion. When the HWRE is operating at 1,000 rpm, 80 kPa MAP and an excess air ratio of 1.0, the FCV is 53 m/s.

BCV is the result of a race between the flow velocity and the flame velocity, so when the flow velocity is faster than the flame velocity, the flame cannot propagate back, i.e., BCV is 0. In this situation, the backward flame propagation is completely determined by the in-cylinder flow field, which is unfavorable for achieving the Otto cycle. Therefore, the developed dual spark plugs are very necessary for WRE, which can be more optimistic to improve the constant volume combustion level, even if the hydrogen fuel has a fast burning speed. When the flame can not propagate backward, the in-cylinder pressure profiles as shown in Fig. 7. In-cylinder pressure changes continuously with TSP ignition timing delay. The in-cylinder pressure may not change during the TSP ignition delay, but as the rotor rotates, the volume of the combustion chamber increases so that the in-cylinder flow field is no longer unidirectional, rather, it appears to be vortex or swirling, leading to errors in combustion velocity measurements. Hence, it can be assumed that when the flame still cannot propagate in the TSP at 15◦CA ATDC, the flame can not propagate backward. Among the cases tested in Fig. 6, only when the HWRE operates at stoichiometric ratio, the BCV is obtained, which is 22.7 m/s. According to equations (1) and (2), the flame velocity and flow velocity can be calculated as 37.85 m/s and 15.15 m/s, respectively. Since flow velocity is affected by both engine speed and MAP, it can be assumed that flow velocity is maintained when neither changes. Therefore, the flame velocity at different excess air ratios can be obtained as shown in Fig. 8. According to Fig. 8 when decoupling the flow velocity, the HWRE flame velocity decreases with the increase of excess air ratio.

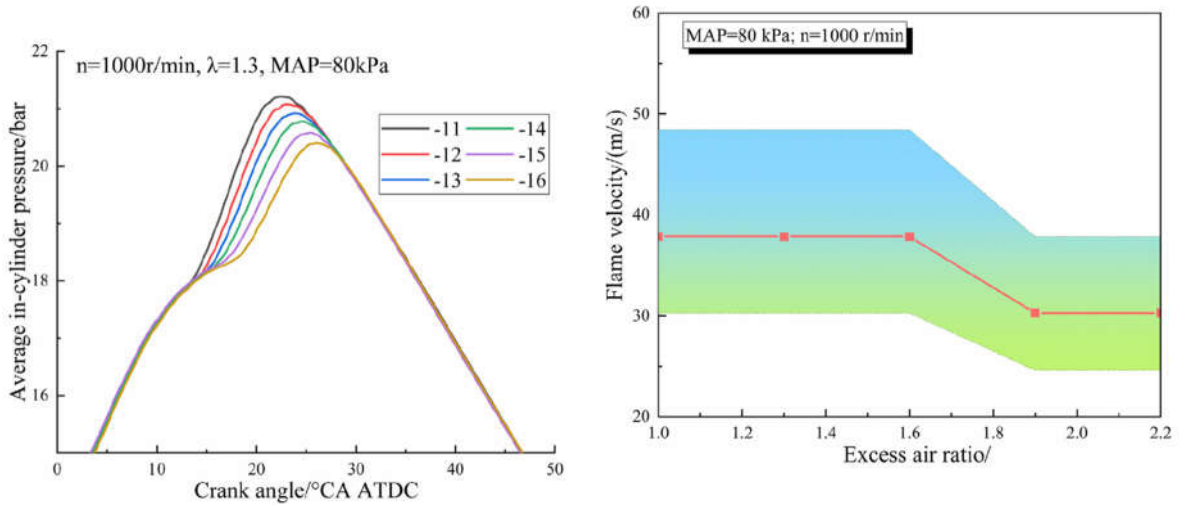

3.2.2. Engine speed

Fig. 9 shows the FCV at different engine speeds, which includes measured data (dotted line) and error band (colored band). It can be seen that FCV increases gradually with increasing engine speed. It may be explained by the following reasons: When the MAP is constant at 80 kPa, the intake kinetic energy is essentially similar. When the excess air ratio is fixed at 1.6, the effect of hydrogen concentration on combustion can also be eliminated. The rotation of the rotor and the shape change of the combustion chamber, including the direction and velocity of the flow field, determine the flow field inside the WRE cylinder. As the rotation speed of the WRE rotor increases, the velocity of the flow field inside the cylinder driven by the rotor also increases. Hence, the FCV with the same flow field direction increases significantly under the influence of increasing engine speed. Furthermore, there is an approximately linear relationship between FCV and engine speed. As the engine speed increases from 1000 rpm to 2500 rpm, the FCV increases from 53 m/s to 79.5 m/s.

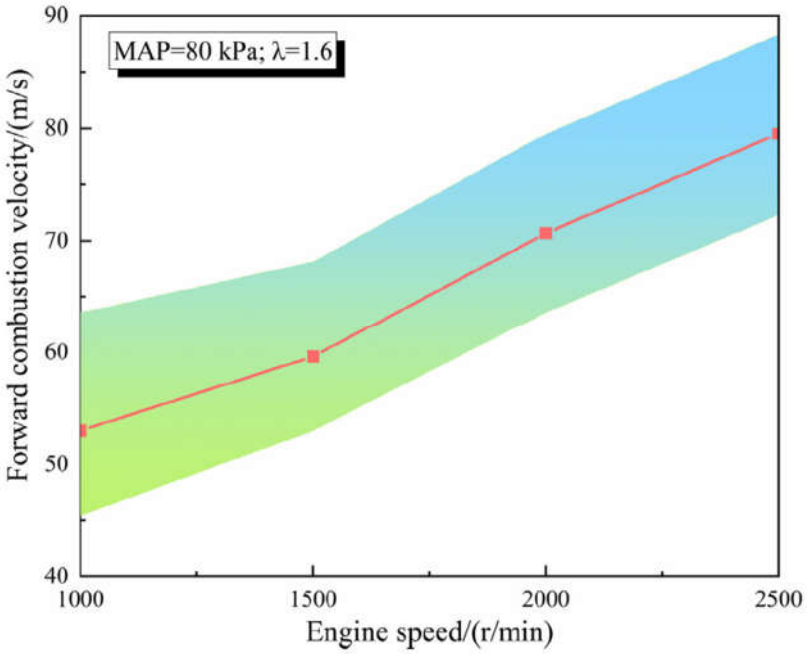


**Fig. 9.** The forward combustion velocity at different engine speeds. [43]

The average velocity of the in-cylinder flow field is determined only by the rotor rotation speed, and there is a linear relationship between the rotor rotation speed and the flow velocity. Therefore, based on the flow velocity measured at 1000 r/min, it is possible to calculate the flow velocities of 1500, 2000 and 2500 m/s, which are 22.7, 30.3 and 37.9 m/s, respectively. Combining with eq (1), the flame velocity at different engine speeds can be obtained, as shown in Fig. 10. When the excess air ratio is constant, there appears to be no significant relationship between flame velocity and engine speed. This may be because the flame velocity is mainly affected by the mixture concentration, therefore, when decoupling the effect of the flow field from the combustion velocity, the difference between the flame velocities at the same charge concentration and different speeds is not obvious.

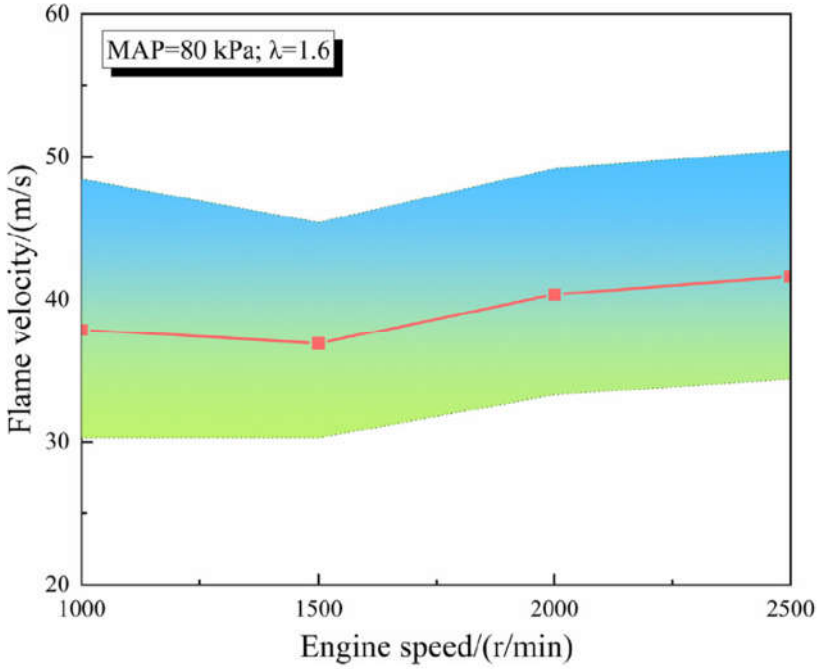


**Fig. 10.** The flame velocity at different engine speeds. [43]

### 3.3. The relationship between knock and combustion, flow and flame velocity

The fitted data were used to complete the plot in Fig. 11, which shows KI at the corresponding fitted forward combustion/flame velocity, to better illustrate the relationship between knock and combustion/flame velocity. It can be seen from Fig. 11 that when the flow velocity is constant, as the FCV velocity or flame velocity increases, the KI gradually increases at an increasing rate rather than a constant rate. After the formation of the flame kernel, the flame front propagates forward stably with a pressure wave ahead. This pressure wave is formed by the temperature gradient between the flame front and the unburned charge, which is positively correlated with the flame velocity. Therefore, when the combustion/ flame velocity increase, stronger pressure waves are generated, thus triggering more intense in-cylinder pressure oscillations, which manifest as high KI. Besides, the non-linear relationship between KI and combustion velocity may suggest the need to control the combustion velocity of HWRE within a suitable range, to ensure a satisfactory constant-volume combustion degree without triggering a violent knock.

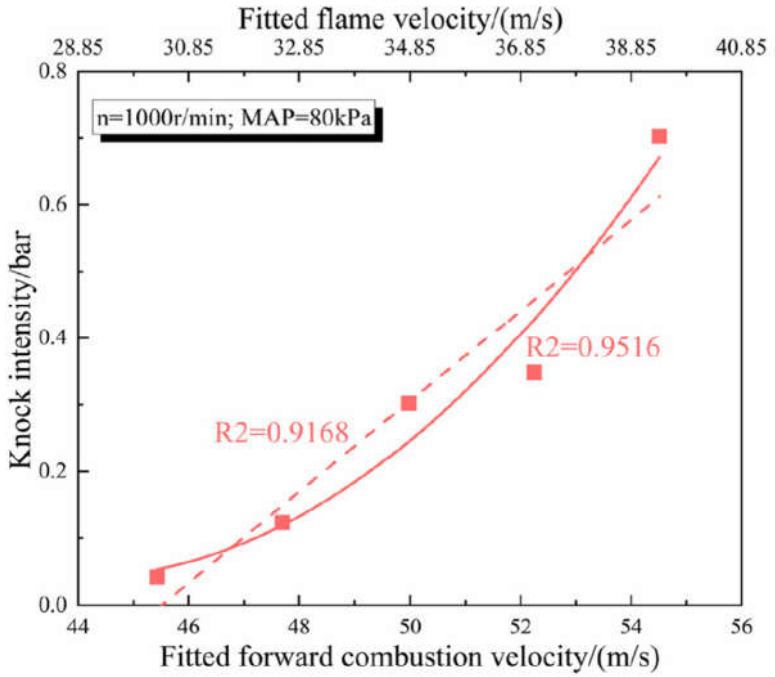


**Fig. 11.** Knock intensity at corresponding fitted forward combustion/flame velocity. [43]

Fig. 12(a) and (b) show the KI at FCV and corresponding flow velocity, respectively, when the flame velocity is similar. KI shows an approximately linear increase with increasing FCV and flow velocity. The reasons for this trend are the same as those described in Fig. 11. It should be noted that the increase of FCV in Fig. 12a is due to the increase of flow velocity while in Fig. 11 it is due to the increase of flame velocity, thus causing a difference in the relationship between KI and FCV. An increase in flame velocity compared to an increase in flow velocity leads to a significant increase in KI. It indicates how important it is to increase in-cylinder turbulence rather than flame velocity to achieve satisfactory constant volume combustion to avoid knocking.

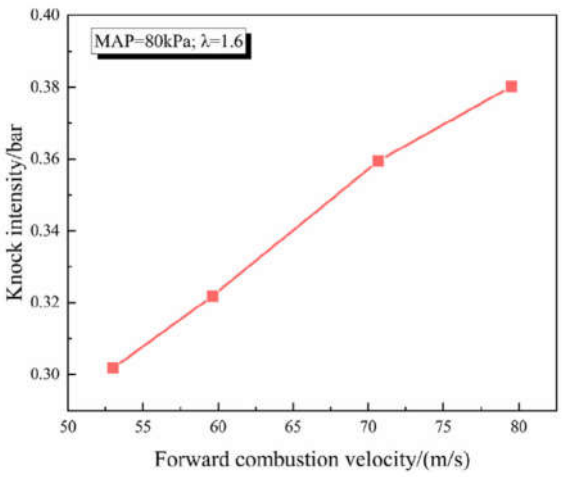


**Fig. 12(a).** Knock intensity at corresponding forward combustion velocity.

Reference [43]

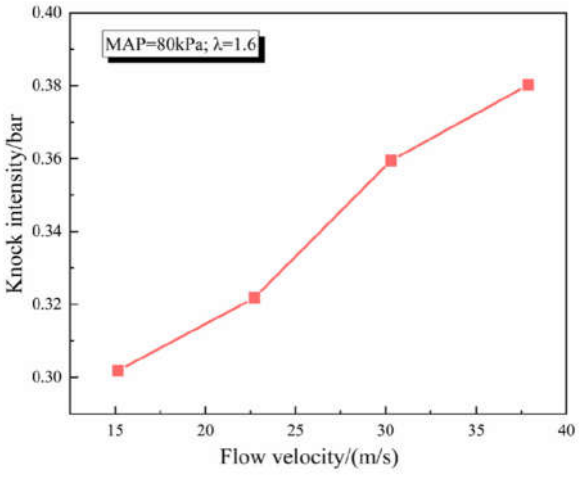


**Fig. 12(b).** Knock intensity at corresponding flow velocity.

Reference [43]

## 4. Conclusions

Based on Wankel rotary engine (WRE) experimental bench, a method for measuring the combustion velocity of hydrogen-fueled WRE is proposed. And the relationship between knock level and combustion velocity in HWRE is quantified.

1. Providing a combustion velocity measuring method of dual spark plug HWRE according to the in-cylinder pressure, which can measure average combustion, flow and flame velocity, for hydrogen and other fueled WRE. The error of this method is influenced by the tested ignition timing interval.
2. Due to the influence of the in-cylinder flow field, the flame can not propagate backward at the vast majority of operating conditions, thus causing the backward combustion to be dominated by the flow field. Thus, to ensure the level of constant-volume combustion, dual spark plugs are requisite for HWRE.
3. In HWRE, as the excess air ratio increases, forward combustion velocity and flame velocity increase gradually. When the HWRE is operating at 1000 r/min, 80 kPa MAP and stoichiometric ratio, the forward combustion velocity is 53 m/s. And as the engine speed increases, the forward combustion velocity and flow velocity increase gradually while the flame velocity is basically constant, which indicates that the flame velocity is mainly affected by the fuel concentration. At 1.6 excess air ratio and 80 kPa, the forward combustion velocity increases from 53 to 79.5 m/s as the engine speed increases from 1000 to 2500 rpm.
4. The HWRE knock level is affected by flame velocity and flow velocity, both of which are positively correlated with knock intensity. The increase of flame velocity is prone to lead to a more violent knock.

Limited by the measurement method, it can only measure the average value of the relevant parameters.

## REFERENCES

[1] Shi C, Ji C, Ge Y, Wang S, Bao J, Yang J. Numerical study on ignition amelioration of a hydrogen-enriched Wankel engine under lean-burn condition. Appl Energy 2019;255:113800. https://doi.org/10.1016/j.apenergy.2019.113800.

[2] Ji C, Meng H, Wang S, Wang D, Yang J, Shi C, et al. Realizing stratified mixtures distribution in a hydrogen-enriched gasoline Wankel engine by different compound intake methods. Energy Convers Manag 2020;203. https://doi.org/ 10.1016/j.enconman.2019.112230.

[3] Fan B, Zeng Y, Pan J, Fang J, Salami HA, Wang Y. Numerical study of injection strategy on the combustion process in a peripheral ported rotary engine fueled with natural gas/hydrogen blends under the action of apex seal leakage. Energy 2022;242:122532. https://doi.org/10.1016/ j.energy.2021.122532.

[4] Meng H, Ji C, Wang S, Wang D, Yang J. Optimizing the idle performance of an n-butanol fueled Wankel rotary engine by hydrogen addition. Fuel 2021;288: 119614. https://doi.org/10.1016/j.fuel.2020.119614.

[5] Shi C, Zhang P, Ji C, Di L, Zhu Z, Wang H. Understanding the role of turbulence-induced blade configuration in improving combustion process for hydrogen-enriched rotary engine. Fuel 2022;319:123807. https://doi.org/10.1016/ j.fuel.2022.123807.

[6] Amrouche F, Erickson PA, Varnhagen S, Park JW. An experimental analysis of hydrogen enrichment on combustion characteristics of a gasoline Wankel engine at full load and lean burn regime. Int J Hydrogen Energy 2018;43: 19250. https://doi.org/10.1016/j.ijhydene.2018.08.110. e9.

[7] Tutu Andrei. Why Mazda decided to cancel the RX-8 successor: goodbye Wankel engine!. 2014. https://www.autoevolution.com/news/why-mazda-decided-to-cancel-the-rx-8-successor-goodbye-wankel-engine-88720.html#: ~:text¼Ever since Mazda pulled the plug on the,automaker wants to discontinue the RX sportscar series.

[8] Gao J, Xing S, Tian G, Ma C, Zhao M, Jenner P. Numerical simulation on the combustion and NOx emission characteristics of a turbocharged opposed rotary piston engine fuelled with hydrogen under wide open throttle conditions. Fuel 2021;285. https://doi.org/10.1016/j.fuel.2020.119210.

[9] Gürbüz H, Akçay _ IH. Evaluating the effects of boosting intake-air pressure on the performance and environmental-economic indicators in a hydrogen-fueled SI engine. Int J Hydrogen Energy 2021;46:28801e10. https://doi.org/ 10.1016/j.ijhydene.2021.06.099.

[10] Wang D, Ji C, Wang S, Yang J, Wang Z. Numerical study of the premixed ammonia-hydrogen combustion under engine-relevant conditions. Int J Hydrogen Energy 2021;46:2667e83. https://doi.org/10.1016/ j.ijhydene.2020.10.045.

[11] Gurbuz H. The effect of H2 purity on the Combustion,Perfomance, emissions, and energy costs in an spark ignition engine. Therm Sci 2020;24:37e49. https://doi.org/10.2298/TSCI180705315G.

[12] Gao J, Tian G, Ma C, Huang L, Xing S. Explorations of the impacts on a hydrogen fuelled opposed rotary piston engine performance by ignition timing under part load conditions. Int J Hydrogen Energy 2021;46:11994. https://doi.org/10.1016/j.ijhydene.2021.01.030. e2008.

[13] Amrouche F, Erickson PA, Park JW, Varnhagen S. Extending the lean operation limit of a gasoline Wankel rotary engine using hydrogen enrichment. Int J Hydrogen Energy 2016;41:14261e71. https://doi.org/10.1016/ j.ijhydene.2016.06.250.

[14] Meng H, Ji C, Xin G, Yang J, Chang K, Wang S. Comparison of combustion, emission and abnormal combustion of hydrogen-fueled Wankel rotary engine and reciprocating piston engine. Fuel 2022;318:123675. https://doi.org/ 10.1016/j.fuel.2022.123675.

[15] Wakayama N, Morimoto K, Kashiwagi A, Saito T. Development of hydrogen rotary engine vehicle. In: 16th world hydrog energy conf 2006. vol. 1. WHEC; 2006. p. 733e8. 2006.

[16] Verhelst S, Wallner T. Hydrogen-fueled internal combustion engines. Prog Energy Combust Sci 2009;35:490e527. https://doi.org/10.1016/ j.pecs.2009.08.001.

[17] Morimoto K, Teramoto T, Takamori Y. Combustion characteristics in hydrogen fueled rotary engine. SAE Tech Pap 1992. https://doi.org/10.4271/920302.

[18] Gao J, Wang X, Song P, Tian G, Ma C. Review of the backfire occurrences and control strategies for port hydrogen injection internal combustion engines. Fuel 2022;307:121553. https://doi.org/10.1016/j.fuel.2021.121553.

[19] Zhen X, Wang Y, Xu S, Zhu Y, Tao C, Xu T, et al. The engine knock analysis - an overview. Appl Energy 2012;92:628e36. https://doi.org/10.1016/ j.apenergy.2011.11.079.

[20] Shi H, Uddeen K, An Y, Pei Y, Johansson B. Statistical study on engine knock oscillation and heat release using multiple spark plugs and pressure sensors. Fuel 2021;297:120746. https://doi.org/10.1016/j.fuel.2021.120746.

[21] Ricardo HR. Recent research work on the internal-combustion engine. SAE Tech Pap 220001 1922. https://doi.org/10.4271/220001.

[22] Corrigan DJ, Fontanesi S. Knock: a century of research. SAE Int J Engines 2021;15:3e15. https://doi.org/10.4271/03-15-01-0004.

[23] Pan J, Shu G, Wei H. Interaction of flame propagation and pressure waves during knocking combustion in spark-ignition engines. Combust Sci Technol 2014;186:192e209. https://doi.org/10.1080/00102202.2013.857665.

[24] Szwaja S, Naber JD. Dual nature of hydrogen combustion knock. Int J Hydrogen Energy 2013;38:12489e96. https://doi.org/10.1016/ j.ijhydene.2013.07.036.

[25] Szwaja S. Knock and combustion rate interaction in a hydrogen fuelled combustion engine. J KONES 2011;18:431e8.

[26] Szwaja S, Naber J. Impact of leaning hydrogen-air mixtures on engine combustion knock. J KONES 2008;15:483e91.

[27] Curry S. A three-dimensional study of flame propagation in a spark ignition engine. SAE Tech Pap 1963:628e50. https://doi.org/10.4271/630487.

[28] Chun KM, Heywood JB. Characterization of knock in a spark-ignition engine. SAE Tech Pap 1989. https://doi.org/10.4271/890156.

[29] Gürbüz H, Buran D. Experimental study on the effect of concentrated turbulence around the spark plug zone in a swirling flow on a hydrogen SI engine performance and combustion parameters. J Energy Eng 2016;142:04015031. https://doi.org/10.1061/(asce)ey.1943-7897.0000297.

[30] Jemni MA, Kassem SH, Driss Z, Abid MS. Effects of hydrogen enrichment and injection location on in-cylinder flow characteristics, performance and emissions of gaseous LPG engine. Energy 2018;150:92e108. https://doi.org/ 10.1016/j.energy.2018.02.120.

[31] Kacem SH, Jemni MA, Driss Z, Abid MS. The effect of H2 enrichment on in-cylinder flow behavior, engine performances and exhaust emissions: case of LPG-hydrogen engine. Appl Energy 2016;179:961e71. https://doi.org/ 10.1016/j.apenergy.2016.07.075.

[32] Spreitzer J, Zahradnik F, Geringer B. Implementation of a rotary engine (Wankel engine) in a CFD simulation tool with special emphasis on combustion and flow phenomena. SAE Tech Pap Ser 2015;1. https://doi.org/ 10.4271/2015-01-0382.

[33] Taskiran OO, Calik AT, Akin Kutlar O. Comparison of flow field and combustion in single and double side ported rotary engine. Fuel 2019;254:115651. https:// doi.org/10.1016/j.fuel.2019.115651.

[34] Shi C, Ji C, Wang S, Yang J, Li X, Ge Y. Numerical simulation on combustion process of a hydrogen direct-injection stratified gasoline Wankel engine by synchronous and

asynchronous ignition modes. Energy Convers Manag 2019;183:14e25. https://doi.org/10.1016/j.enconman.2018.12.081.

[35] Fan B, Pan J, Liu Y, Chen W, Lu Y, Otchere P. Numerical investigation of mixture formation and combustion in a hydrogen direct injection plus natural gas port injection (HDI þ NGPI) rotary engine. Int J Hydrogen Energy 2018;43: 4632e44. https://doi.org/10.1016/j.ijhydene.2018.01.065.

[36] Meng H, Ji C, Yang J, Chang K, Xin G, Wang S. Understanding the relationship between knock and heat release in hydrogen-fueled Wankel rotary engine(- submitted). Int J Hydrogen Energy.

[37] Yang J, Meng H, Ji C, Wang S. Comparatively investigating the leading and trailing spark plug on the hydrogen rotary engine. Fuel 2022;308:122005. https://doi.org/10.1016/j.fuel.2021.122005.

[38] Fan B, Zeng Y, Pan J, Fang J, Hammed AS, Wang Y. Evaluation and analysis of injection strategy in a peripheral ported rotary engine fueled with natural gas/ hydrogen blends under the action of apex seal leakage. Fuel 2022;310: 122315. https://doi.org/10.1016/j.fuel.2021.122315.

[39] Brunt MFJ, Pond CR, Biundo J. Gasoline engine knock analysis using cylinder pressure data. SAE Tech Pap 1998. https://doi.org/10.4271/980896.

[40] Meng H, Ji C, Su T, Yang J, Chang K, Xin G, et al. Analyzing characteristics of knock in a hydrogen-fueled Wankel rotary engine. Energy 2022;250:123828. https://doi.org/10.1016/j.energy.2022.123828.

[41] Lounici MS, Benbellil MA, Loubar K, Niculescu DC, Tazerout M. Knock characterization and development of a new knock indicator for dual-fuel engines. Energy 2017;141:2351e61. https://doi.org/10.1016/j.energy.2017.11.138.

[42] Ko YS, Chung SH. Propagation of unsteady tribrachial flames in laminar non-premixed jets. Combust Flame 1999;118:151e63. https://doi.org/10.1016/ S0010-2180(98)00154-0.

[43] Meng H, Ji*C, Yang J, Chang K, Xin G, Wang, Experimental understanding of the relationship between combustion/ flow/flame velocity and knock in a hydrogen-fueled Wankel rotary engine. Energy 2022;258;124828 https://doi.org/10.1016/j.energy.2022.124828